Chapter 3

Internalisation of Rafts

We have seen that domains on the exoplasmic leaflet of the plasma membrane, rich in cholesterol and sphingolipids, bear dense and tiny clusters of GPI-anchored proteins at the nanometre scale. We also know that components of 'rafts', as these domains are called, are internalised by the cell along a path that does not intersect the path of clathrin-mediated endocytosis at all (recall section 1.3).

As discussed in the section 1.3, the major difference between the 'raft-mediated' and the clathrin-mediated pathways, is that the former path of entry into the cell does not involve the vast troop of membrane deforming proteins including the cytosolic coat protein, clathrin, and GTP-ases like dynamin. Dynamin and other GTP-ases can exert forces on the coated pit either by allosteric modification of the structure of the protein itself or by reorganising cytoskeletal fibres around the pit and linking motor proteins that tread on the fibres with proteins embedded in the pit. Neither any coat nor any large GTP-ase like dynamin has been observed to be associated with rafts. So we shall work on the premise that the membrane of the raft itself, owing to the special composition of lipids, is deforming the surface of the cell to trigger the process of endocytosis, without any help or impediment from the cell cortex.

The endocytosis of rafts is a *constitutive* process, no external agent signaling its commencement — the signal must be in the special environment on the exoplasmic leaflet created by cholesterol and sphingolipids. Though GPI-anchored proteins find themselves clustered in rafts, it is the special milieu of lipids in the raft rather than the clustering of proteins that lead to the new endocytic pathway. If a certain species of GPI-anchored protein is crosslinked by an antibody then the induced cluster fails to be endocytosed along the new pathway, the crosslinked species enters the cell through clathrin-coated pits. In this chapter we search for a mechanism of endocytosis based entirely on the lipid composition of the membrane absorbed by the cell. In the fifth section we ask: is there any domain of the cell, other than rafts, where a similar composition of lipids is encountered? The answer is Yes, in *caveolae.* Our theory not only suggests a plausible mechanism of the endocytosis of rafts but also explains the unique morphology of caveolae.

3.1 Ways to form a bud

We discuss three ways, not mutually exclusive, in which a lipid domain with a sharp boundary on the outer leaf of a fluid bilayer membrane can form a bud.

3.1.1 Budding induced by line tension

The energy of a macroscopic domain of a fluid membrane of area $A (= \pi R^2)$ and perimeter L can be expressed as

$$\mathrm{E} = \sigma_0 L + \frac{\kappa}{2} \int_A (c - c_0)^2 \tag{3.1}$$

σ_0 is the line tension and κ the elastic modulus for bending deformations (Lipowski; 1992). c_0, the spontaneous curvature of the membrane, is a measure of the dissimilarity in the composition of the two leaves of the bilayer forming the domain. c, the mean curvature, takes the value $\frac{1}{r}$ for a domain in the shape of a part of a sphere of radius r. Let us ignore c_0 for the moment, then the energy of a plane domain is $E_{plane} = 2\pi\sigma_0 R$, while that of a spherical domain will be $E_{bud} = 2\pi\kappa$ (L = 0). Therefore if R exceeds a threshold, r_{bud}, then E_{bud} becomes smaller than E_{plane}, and as a result, the domain will form a bud.

$$r_{bud} = \frac{\kappa}{\sigma_0} \tag{3.2}$$

The value of κ has not been measured for the plasma membrane; but it must be of the order of 10^{-12} erg. Meleard and his collaborators have studied the effect of cholesterol on the bending elasticity of artificial membranes by creating giant (20 micron diameter) quasispherical vesicles and observing, by phase-contrast video microscopy, the spontaneous wriggling of the vesicles due to thermal fluctuations (Meleard et al; 1997). The statistical properties of the wriggling shapes are governed by only two characteristics of the membrane — κ and the surface tension. By comparing their theoretical picture of the shape deformations with the experimental results they have arrived at the best-fitting value of κ — at 40° C, $\kappa = 3 \times 10^{-12}$ erg for a 30 mole per cent mixture, and $\kappa = 4 \times 10^{-12}$ erg for a 50 mole per cent mixture of cholesterol in DMPC. Interestingly, they have also noticed that the value of κ is insensitive to the presence of electric charges on the lipids.

The energy of thermal agitation at T = 40° C is $k_B T \approx 4 \times 10^{-14}$ erg. $\kappa >> k_B T$, therefore deformations of the membrane due to thermal fluctuations are utterly insignificant in the process of budding.

The line tension of a domain formed by microphase separation in a lipid bilayer membrane has not been measured. However we can borrow the results of observations on a langmuir monolayer (a film of insoluble amphiphilic molecules at the air-water interface) composed of a long chain fatty acid. Riviera and his collaborators have studied the shape deformations of a liquid domain in the monolayer surrounded by a less dense liquid (Riviere et al; 1995). The deformation is because of the electrical attraction between the dipoles of the domain with those of a neighbouring domain — by recording the surface

potential of the monolayer they have been able to deduce the strength of the electrical attraction. And the line tension of the domain resists the electrical pull. These opposite tendencies dictate the shape of the domain, hence observing the shape of the domain by fluorescence microscopy, they arrive at an estimate of the line tension, $\sigma_0 \sim 10^{-8}$ dyne.

Baumgart and his coworkers have produced giant unilamellar vesicles in which liquid-ordered domains, rich in cholesterol and sphingolipids, coexist with liquid-disordered patches consisting mainly of unsaturated phospholipids (Baumgart et al; 2003). Recording the shapes of the domains in axisymmetric vesicles, they have been able to calculate the line tension, σ_0, by comparing the shapes they obtain with those predicted by theory (Julicher and Lipowski; 1996). Their best-fitting value of σ_0 concurs with the value measured on a monolayer.

Plugging the numbers we have gleaned into Equation 3.2, we arrive at $r_{bud} \sim 1\mu$m. Since the dimension of clathrin-coated pits and of rafts in living cells are around 50 nm (and certainly smaller than 100 nm), clearly, we have to seek a different mechanism to understand the process of internalisation of rafts from the plasma membrane.

3.1.2 Budding induced by spontaneous curvature

The inherent asymmetry of the cytosolic and the exoplasmic layers of a raft may induce the membrane to deform. The transverse asymmetry could be due to (i) differences in lipid composition (recall that sphingolipids are present only in the outer leaf), (ii) the presence of a cortex on one side of the cell surface or (iii) the recruitment of cytosolic proteins onto the lower leaf of the plasma membrane. Furthermore, the gross shape of the molecular constituents of the membrane, crudely dictated by the ratio of the cross-sectional areas of the hydrophilic part and the hydrophobic part of the molecule also contributes to the spontaneous curvature of the membrane. Recently, Sens and Turner have suggested that the protein *caveolin,* known to be associated with caveolae, generates forces on the lower leaf of the membrane, leading to an effective spontaneous curvature (Sens and Turner; 2003). However, the sizes of buds their theory predicts ($\sim$ 1pm) are still too large to account for the existence of the structures found at the plasma membrane.

3.1.3 Budding induced by chirality

Let us, for the moment, treat the lipid bilayer membrane as a plane and the raft as a circular patch of constant area residing on the plane. We will argue in the next section that the special constitution of rafts, namely cholesterol and sphingolipids, allows for a decoration of the circular patch by a vector field possessing chirality. For now, let us imagine that every point within the circle is associated with a vector of unit magnitude. If the vector field possess sufficient strength of chirality then it will take the form of an Archimedes spiral, diverging from C, the centre of chirality, and everywhere subtending half a right angle with respect to the local radial. C is a defect core and the chiral

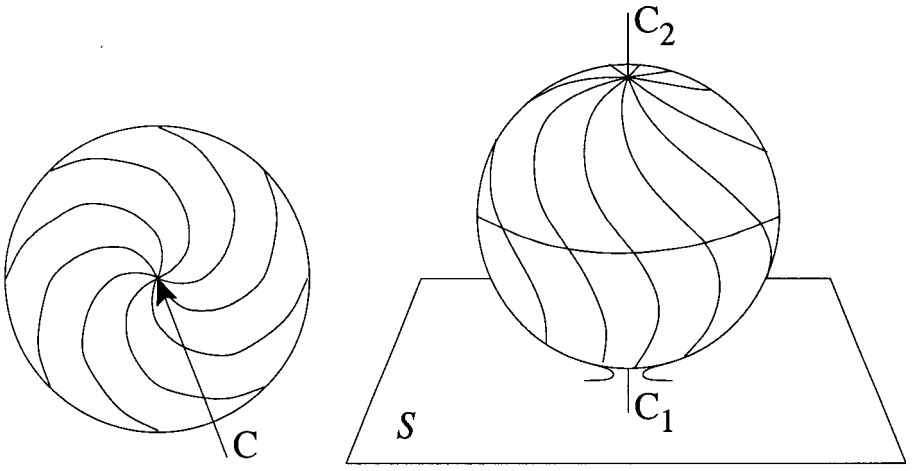

Figure 3.1: (L) Chiral texture on a flat membrane, the plane of the paper; C is the centre of chirality. (R) A spherical bud induced by chirality, connected to the plane S by an infinitesimal neck; C_1 and C_2 are centres of chirality.

interaction is strongest at that point, falling off inversely as the square of the distance from C. Therefore, if the plane be deformable, then the spiral can close itself on the opposite pole of a sphere, producing two centres of chirality, C_1 and C_2, instead of one. Thus a spherical bud is produced if the chirality of the vector field be sufficiently strong to overcome the rigidity of the membrane.

Why does the raft on the plane not split into two, each with a spiral texture, thus forming two centres of chirality, instead of bulging out in the form of a sphere? It is a property of chiral systems to abolish mirror symmetry. The Archimede's spiral is not symmetric with respect to reflection on any mirror except one — the mirror that coincides with the plane of the raft. A chiral object can not be made to lie on a plane. Not only the spiral, a helix is also a texture favoured by chirality. In fact a look at Figure 3.1 will convince the observer that the spiral texture on the sphere is equivalent to one pitch of a deformed helix — imagine a pitch of a helix drawn on a cylinder of radius r and length $2r$, where r is the radius of the spherical bud; now squeeze the ends of the cylinder till they shrink to points, leaving the middle of the cylinder unchanged — the resulting texture is indeed what has been shown in Figure 3.1.

We now understand that chirality does indeed force a raft on a plane into the shape of a spherical bud.

3.2 Vector fields to decorate a raft

In the previous chapter we have seen that GPI-anchored proteins with different ectodomains, but not transmembrane isoforms of those proteins, inhabit the same nanocluster. Therefore the clusters are formed by lipid-based mechanisms. We can take one step further to assert that not only proteins with sphingolipid tethers, but sphingolipids themselves form clusters in conjunction with cholesterol. Let us call these lipid clusters *condensed*

complexes. If an individual condensed complex is composed of only a few molecules (like a protein cluster) so that it is not big and circular in shape, then we can assign a vector to each condensed complex to represent an axis fixed to the body of the complex. Assuming that the rotational diffusion of the condensed complexes in a raft is hindered, the time-averaged projection of the body-fixed axis on the plane of the membrane is non-vanishing. We shall assume that the density of the complexes in a raft is constant, as a result the magnitude of the vector field at every point of the raft is also a constant.

Though we have to be cautious in applying the results of studies on artificial systems to understand the membrane of a living cell, it is worthwhile noting that the presence of condensed complexes has been inferred from a knowledge of the phases in which a monolayer of cholesterol and chosen lipids can exist at the air-water interface (Radhakrishnan et al; 2000). Epifluorescence microscopy of mixtures of lipids and cholesterol often exhibit three coexisting fluid phases: a lipid-rich phase, a cholesterol-rich phase and a condensed complex-rich phase. To understand the composition of the condensed complex, a theoretical model has been constructed of a ternary mixture of cholesterol C, and two lipids, S and U (Anderson and McConnell; 2002). S refers to lipids such as sphingolipids or phosphatidylcholines with long saturated fatty acid chains that form complexes with cholesterol. U is a lipid such as a phosphatidylcholine with unsaturated fatty acid chains that does not form complexes. (Phosphatidylcholines with saturated but short chains also do not form complexes.) C and S undergo a reversible reaction to form a complex:

$$nqC + npS \leftrightarrow C_{nq}S_{np} \tag{3.3}$$

n is the degree of oligomerisation and p, q are relatively prime numbers indicating the stoichiometry of the condensed complex. Theory agrees with observed phase diagrams for $p = 2$, $q = 1$, and n varying from 3 to 10.

Thus an artificial lipid monolayer spawns condensed complexes with as many as 15 to 30 molecules in an individual complex. However, given the evidence of nanoscale clusters of GPI-anchored proteins, we believe that in a raft on a living cell, the condensed complexes will be much smaller, enabling us to decorate the raft with a vector field where the vector at each point is a coarse-grained picture of the axes fixed to the complexes around that point.

We propose another vector field to decorate the raft. Unlike the field described in the previous paragraph, this vector owes its origin to the structural features of individual lipid molecules forming the raft. In the special environment of the raft, the saturated fatty acid chains of a constituent lipid could assume the all-cis configuration, thus becoming rigid. Along the frozen chains of such a lipid molecule one can draw a vector aiming toward the head group. The projection of that vector on the plane of the membrane could serve as the field with a chiral interaction.

There are essentially two possible origins of chiral interactions between molecules. The

first is quantum mechanical and best thought of as a generalisation of the van der Waals dispersion to chiral molecules. The electrostatic potential between a pair of molecules is expanded to include dipole-quadrupole as a well as dipole-dipole interactions. This leads to a 2-body intermolecular potential of the form

$$V_{chiral} \propto \frac{(\vec{e}\cdot\vec{e'})(\vec{e}\cdot(\vec{R}\times\vec{e'})}{|\vec{R}|^7} \tag{3.4}$$

where Band $\vec{e'}$ are unit vectors along the chosen principal axes of the molecules separated by $\vec{R}$. The second mechanism can be described in classical terms, arising from central force potentials (including hard-core repulsion) between atoms constituting chirally shaped molecules. Imagine a collection of screws arranged along a line. At low densities these chiral "molecules" are free to rotate about any axis and so chirality does not propagate over large scales. On increasing density, the "molecules" interact: the interlocking screws twist relative to one another, the protrusion of one fitting into the notch of the other, resulting in an increased packing density. This mechanism can transmit molecular chirality over large scales resulting in a macroscopic structure which is chiral.

Is it not an astonishing fact that of the 256 enantiomers, corresponding to 8 chiral centres in a cholesterol molecule, exactly one occurs naturally in a living cell? Condensed complexes do form in artificial systems with different enantiomers of cholesterol; it seems plausible to us that a pure chiral species of cholesterol in a raft is the agent transmitting chirality over macroscopic scales (Sarasij et al; 2004). Or it could be that the source of chirality is in the shape of the condensed complexes, molecular chirality of cholesterol enhancing the strength of the chiral interaction among the complexes.

3.3 Energy of the raft

Though the system of rafts embedded in the cell membrane need not be in thermodynamic equilibrium we shall assume that a single raft, imagined to be a stable circular region of area A on the membrane, attains a conformation minimising the free energy of that single raft. This assumption tacitly entails another: the fluctuations in the size of the raft due to molecules leaving the raft and entering it from the surrounding membrane are small compared to A. Furthermore, all macroscopic quantities associated with the raft, such as its energy, its texture, or its shape, are evaluated not at a single instant of time but are averaged over a period long compared to the time scale of fluctuations in A.

We shall henceforth treat a raft as a region of perimeter L drawn with a sharp boundary on a mathematical surface. Our aim is to understand the nature of budding induced by chirality; we shall simplify the system and focus especially on chirality. We shall ignore the spontaneous curvature of the raft and take the energy of the system to be

$$E = \sigma_0 L + \int_A (\frac{\kappa}{4}(K_i^i)^2 + \frac{k_1}{2}(\mathbf{div}\vec{m})^2 + \frac{k_2}{2}(\mathbf{curl}\vec{m})^2 + k_c(\mathbf{div}\vec{m})(\mathbf{curl}\vec{m}) + c_0^*\gamma_{ij}m^k m^i K_k^j) \tag{3.5}$$

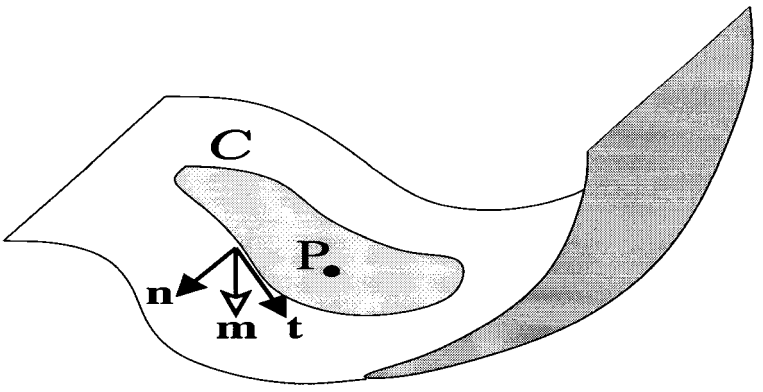

Figure 3.2: Definition of the divergence and the curl of a vector field $\vec{m}$ at the point P on a curved surface.

where K is the curvature of the surface and γ is the completely antisymmetric tensor defined on that surface. The meaning of these tensors as well as the full expression of the energy will be elucidated in an appendix; here we shall illustrate the effect of chirality through a few examples.

There is no difficulty in extending the definition of divergence (div) and curl (curl) for a planar vector field $\vec{m}$ to the case when $\vec{m}$ is defined on a curved surface. For calculating div m and curl m at a point **P,** we draw a small circuit, C, around **P** (Figure **3.2).** C is labeled at every point by two vectors, $\vec{t}$ and $\vec{n}$. $\vec{t}$ is tangent to C and $\vec{n}$ is perpendicular to $\vec{t}$, always aiming away from **P,** both being on the surface. Let Δl be the perimeter of C and δl an element of it, then div m and curl m are obtained in the limit of C shrinking to the point **P** as follows:

$$\mathrm{div\,m} = \lim_{\Delta l \to 0} \frac{1}{\mathrm{AA}} \oint_C \delta l(\vec{m} \,.\, \vec{n}) \tag{3.6}$$

$$\mathrm{curl\,m} = \lim_{\Delta l \to 0} \frac{1}{\mathrm{AA}} \oint_C \delta l(\vec{m} \cdot \vec{t}) \tag{3.7}$$

where ΔA is the area of the surface enclosed by C.

Obviously, for a two-dimensional vector field **G,** curl m is a scalar, not a vector. In fact it is a pseudo-scalar because its sign depends on whether the tangent $\vec{t}$ traverses the circuit C in a clockwise or in a counter clockwise sense.

Unfortunately, the values of the coefficients, k_1, k_2, k_c and c_0^* have not been determined for a lipid bilayer membrane, nor for a langmuir monolayer. So we are forced to surmise their orders of magnitude from studies of bulk liquid crystals. In a cholesteric liquid crystal the director field, $\vec{n}$, (aiming locally along the average orientation of the axes of the constituent rod-like molecules) has a helical conformation (Figure 3.3). One can imagine the bulk of a cholesteric to be sectioned into parallel planes, $\vec{n}$ at every point of a plane being parallel to one another while $\vec{n}$ at successive sections gradually twisting around a fixed axis perpendicular to the planes (de Gennes and Prost; 1993). The energy

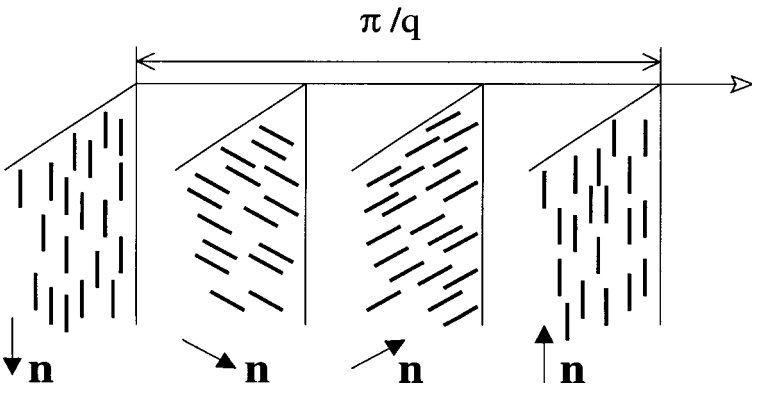

Figure 3.3: Helical conformation of the director n of a cholesteric liquid crystal (de Gennes and Prost; 1993).

density of this system is given by the Frank expression

$$\mathcal{E} = \frac{K_1}{2}(\mathbf{divn})^2 + \frac{K_2}{2}(\mathrm{n.curln} + q)^2 + \frac{K_3}{2}(\mathbf{n} \times \mathbf{curln})^2 \tag{3.8}$$

where $2\pi/q$ is the pitch of the helical conformation of $\vec{n}$. (This formula for $\mathcal{E}$ is valid when the pitch is much larger than the length of the molecule.)

Comparing the energy density of a raft with that of a cholesteric, we set

$$k_1 \sim aK_1 \tag{3.9}$$

$$k_2 \sim aK_3 \tag{3.10}$$

where the length scale a is of the order of the thickness of the bilayer bearing the raft. Since the second term in E has a part varying linearly with curl n therefore we assume that

$$k_c \sim aK_2 \tag{3.11}$$

It is known that $K_1 \sim K_2 \sim K_3 \sim 10^{-6}$ dyne. Taking a $\sim 10\mathring{A}$, we arrive at the estimate $k_1 \sim k_2 \sim k_c \sim 10^{-13}$ erg. Since k_1, k_2 and k_c are almost an order greater than k_BT at 30° C, we may ignore the effect of thermal agitation on the ordering of $\vec{m}$ in a raft.

We still have to take into account the electrical forces in a raft arising from the charges and dipole moments associated with the hydrophilic groups of the constituent lipids. Sphingolipids are zwitterions, as part of a membrane in water, their head groups carry a dipole moment $(\vec{p})$ of magintude $|\vec{p}| \sim 1$ debye $= 10^{-18}$ esu · cm (Israelachvili; 1998). $\vec{p}$ is almost parallel to the plane of the membrane and is at the same level as the bridge group (almost touching the interface of the hydrocarbon chains and water). The strength of interaction of neighbouring sphingolipids is of the order $|\vec{p}|^2/a^3$ where a $\sim 10\mathring{A}$ is the separation of the lipid dipoles. This energy is of the order of 10^{-15} erg, as a result, dipolar interactions can not challenge the order imposed on $\vec{m}$ by the Frank parameters k_1, k_2 and k_c. But if there be a lipid with a net charge q in the raft (usually in the form of the anion O^- in the phosphate radical of the bridge group; GPI-anchored proteins too are

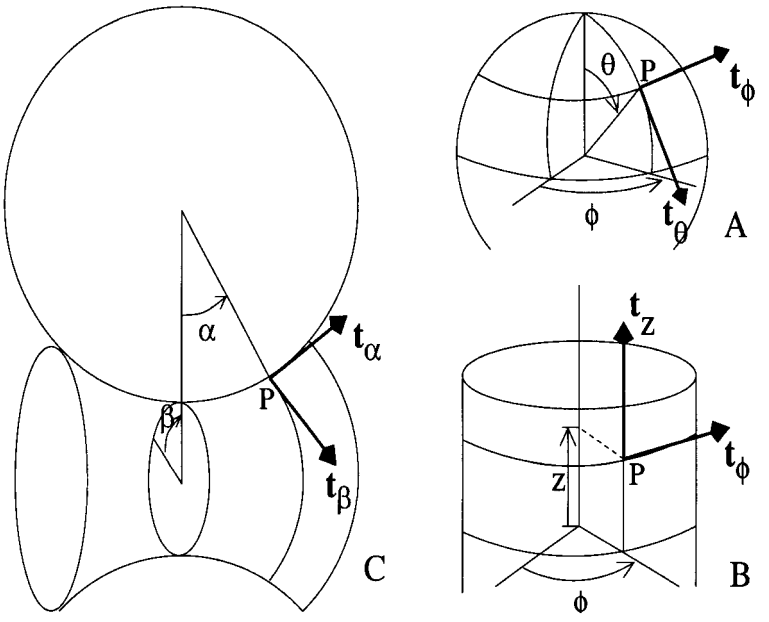

Figure **3.4:** Defining the local coordinate systems on three elementary surfaces (L) a saddle (RT) a sphere (RB) a cylinder.

negatively charged), then the strength of electrical interaction is considerably enhanced. The electrical energy is now of the order $|\vec{p}|q/a^2 \sim 10^{-13}$ erg for q $\approx$ 4 x 10^{-10} esu and $a \approx 8\mathring{A}$. Now the charged lipid would draw the dipoles around itself and arrange them into a shield where each dipole aims radially into the charge, impairing the order of $\vec{m}$ created by the Frank parameters. However, this charge-dipole interaction can be weaker than expected, depending on the pH of the surrounding medium and the nature of dissolved counter ions — factors we have ignored in our analysis. In the rest of this chapter we shall assume that the conformation of the raft is dictated solely by the Frank parameters — it is the conformation (the shape and the texture) that minimises the Frank energy for a given area $\boldsymbol{A}$ of the raft.

Our aim then is to find that conformation. We shall take the variational approach (guessing the right conformation, expressing it in a few parameters, and obtaining the optimal values of the parameters). In some cases our guesses will be educated by computer simulations but primarily our guesses are based on intuition and a general understanding of chiral structures.

Let us so set our units of length and energy that

$$k_1 = 1 \tag{3.12}$$

$$\sigma_0 = 1 \tag{3.13}$$

As a result, the unit of length of our choice becomes $k_1/\sigma_0 = 10^{-5}$ cm, and in these units, the elastic modulus of bending, $\kappa \sim 10$, and thermal energy $k_BT \sim 1$. In what follows we have set $k_2 = 1$, but k_c and c_0^*, the measures of chirality, are variable parameters. One of the features that distinguish the chiral from the achiral terms in the energy of the

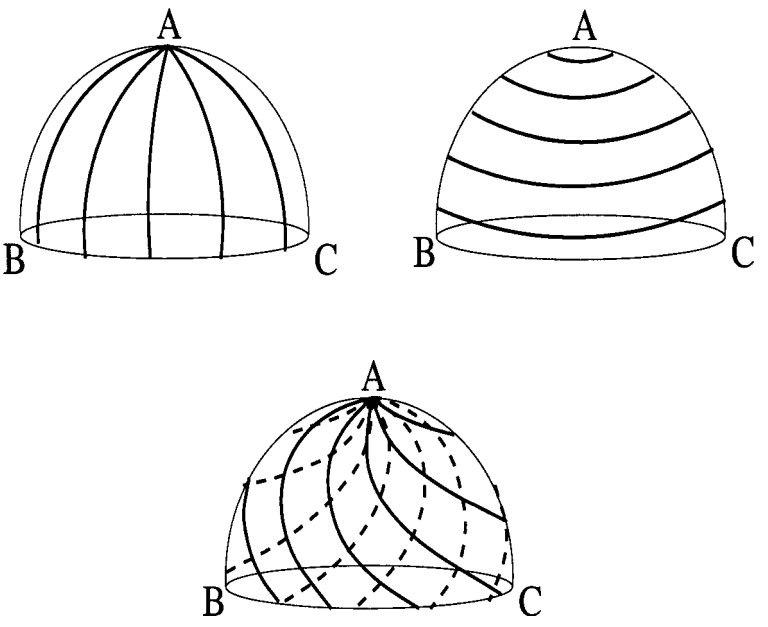

Figure *3.5:* Textures (solid lines) on a sphere and their reflection (broken lines) on a mirror that lies on the plane of the paper (containing the arc BAC).

raft is that the sign of the chiral terms depend on which side of the surface bearing the raft is called "inside" and which is "outside", because the direction of $\vec{N}$, the local normal, and hence the sign of **curl** m, as well as the sign of K_i^j, the local curvature, depends on our definition of "outside" and "inside". We do not know how the asymmetric situation of the raft on the plasma membrane (the cytosol and the cytoskeleton being inside and the exoplasmic fluid outside) affects the sign of the chiral terms in the Frank expression; we shall arbitrarily set $\vec{N}$ everywhere aiming toward one side of the raft and call that side the "outside".

We shall now illustrate the meaning of the chiral terms in a few simple cases. We shall see how these terms lead to textures on a surface that can never be made to coincide with its mirror image no matter where we place the mirror. Any small chip off a surface can be approximated by a plane, a sphere, a cylinder or a saddle (Spivak; 1970). For the moment we shall ignore the plane because a chiral object can not lie on a plane. (Notice that none of these elementary surfaces is chiral.) Naturally, we shall so place the mirror that the bare surface (stripped off its decoration, m) coincides with its reflection. Then we shall decorate the surface, looking for a texture that maximises the contribution of the chiral terms.

Let us start with the sphere. Any point on it is specified by the colatitude θ and the longitude ϕ (Figure 3.4). The tangent plane at any point on it is framed by the unit vectors $\vec{t_\theta}$ (along the direction of increasing 6 and constant ϕ) and $\vec{t_\phi}$ (along the direction of increasing ϕ and constant 6). The texture at any point is defined by

$$\mathbf{m} = m_\theta \mathbf{t}_\theta + m_\phi \mathbf{t}_\phi \tag{3.14}$$

$$m_\theta^2 + m_\phi^2 = 1 \tag{3.15}$$

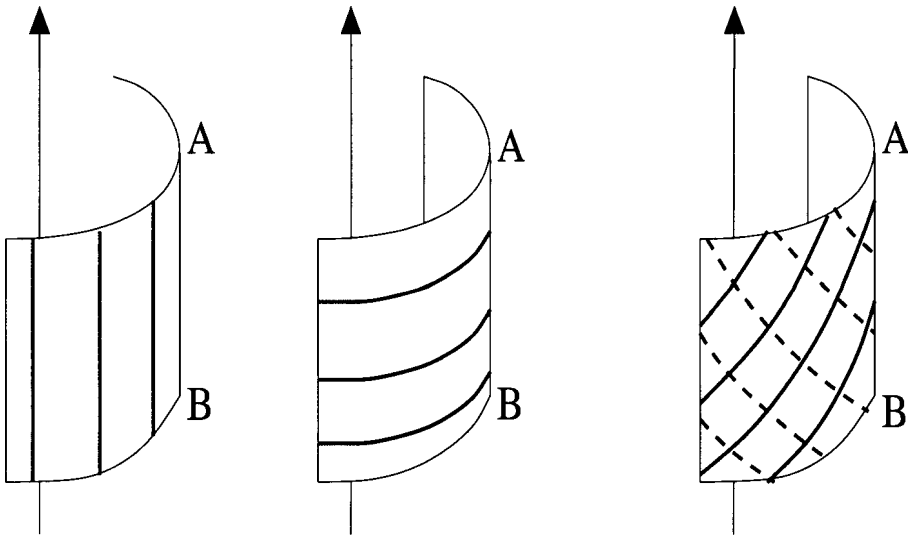

Figure 3.6: Textures (solid lines) on a cylinder and their reflection (broken lines) on a mirror that lies on the plane of the paper (containing the axis and the edge AB).

Any mirror passing through the centre will leave the sphere unchanged after reflection, let us place the mirror along the arc BAC where A is the pole ($8 = 0$, Figure 3.5). If the texture consists of lines parallel to the equator ($m_\theta = 0$, $m_\phi = 1$) or if it consists of great circles diverging from the pole ($m_\theta = 1$, $m_\phi = 0$) then its mirror image coincides with itself. Under these conditions we expect no contribution from the chiral terms. But if the texture consists of lines obliquely cutting the circles of latitude and longitude everywhere on the globe then it is impossible to superpose its mirror image on itself. In fact we expect the chiral term to be greatest when the lines at every point bisect the right angle formed by the intersection of the circles of latitude and longitude, because under this condition the lines of the image will deviate most strongly from the lines in the original texture (they will cut each other at right angles). Indeed that is the case — we calculate the contribution of chirality:

$$c_0^* \gamma_{ij} m^i m^k K_k^j = 0 \tag{3.16}$$

for any texture on the sphere; and taking m_θ and m_ϕ to be constant, we get

$$k_c(\text{divm})(\text{curlm}) = k_c(\frac{\cot\theta}{r})^2 m_\theta m_\phi \tag{3.17}$$

where r is the radius of the sphere. The term vanishes when either m_θ or m_ϕ vanishes, and is greatest when $m_\theta = m_\phi = 1/\sqrt{2}$, confirming our guess.

Now we turn to textures on a cylinder. Every point on the cylinder is specified by its altitude z from a reference plane perpendicular to the axis of the cylinder and by its longitude ϕ from a reference plane containing the axis (Figure **3.4).** The tangent plane at any point of the cylinder is defined by the unit vectors $\vec{t_z}$ (along increasing z, ϕ being constant) and $\vec{t_\phi}$ (along increasing ϕ, z being constant). The texture is

$$\mathbf{m} = m_z \mathbf{t_z} + m_\phi \mathbf{t}_\phi \tag{3.18}$$

$$m_z^2 + m_\phi^2 = 1 \tag{3.19}$$

The surface will not be changed by reflection along any mirror on which lies the axis, let us place our mirror on the plane of the paper, containing the axis and the line AB on the cylinder (Figure 3.6). (The following argument, if repeated with the mirror held perpendicular to the axis, leads to exactly the same conclusion.) Obviously, if the texture consists of lines parallel to the axis (m, $= 1, m_\phi = 0$) or perpendicular to it (m, $= 0$, $m_\phi = 1$) then its mirror image is inseparable from itself. For these textures we expect chirality to have no effect. The chiral term should be greatest when the lines are inclined to the axis at half a right angle because under that condition the lines of the image concur least with those of the original (they cut each other at right angles). Calculations fully support our guess. Taking m, and m_ϕ to be constant,

$$k_c(\mathbf{divm})(\text{curlm}) = 0 \tag{3.20}$$

and

$$c_0^* \gamma_{ij} m^i m^k K_k^j = c_0^* (\frac{1}{r}) m_z m_\phi \tag{3.21}$$

where r is the radius of the cylinder. The term vanishes if either component of m vanishes, and is maximum when m, $= m_\phi = 1/\sqrt{2}$. Observe that the texture with equal and constant components of m is a helix, and that the chiral term is inversely proportional to r. Therefore a large value of c_0^* would wrap m in a helix around a narrow tube, the pitch of the helix being proportional to the radius of the tube. The same effect of molecular chirality on the shape of tilted fluid bilayer membranes, anisotropic solid membranes and ferroelectric liquid crystals has been described by Helfrich and Prost (Helfrich and Prost; 1988).

Like a cylinder, a saddle too has an axis of symmetry, we choose a plane $\mathcal{P}_\alpha$ bearing the axis and place the mirror on it. Unlike a cylinder, however, not any plane perpendicular to the axis is a plane of symmetry for the saddle: there is only one such plane, call it $\mathcal{P}_\beta$. B is the point on the saddle common to $\mathcal{P}_\alpha$ and $\mathcal{P}_\beta$ (Figure 3.7). The other common point, opposite to B, is on the half of the saddle not shown in the figure. For simplicity we shall assume that the lines of intersection of the surface with $\mathcal{P}_\alpha$ and $\mathcal{P}_\beta$ are circles: call them C, and $\mathcal{C}_\beta$ respectively. Any point on the surface is specified by a and β, angles of rotation measured from fixed reference points over C, and $\mathcal{C}_\beta$ respectively (Figure 3.4). (For instance, $\alpha = 0$ at any point on $\mathcal{C}_\beta$, and likewise any point on $\mathcal{C}_\alpha$ has a fixed value of β.) In tune with our method of defining the tangent plane, we construct unit vectors $\vec{t_\alpha}$ and $\vec{t_\beta}$ and describe the texture on the saddle as

$$\mathbf{m} = m_\alpha \mathbf{t}_\alpha + m_\beta \mathbf{t}_\beta \tag{3.22}$$

$$m_\alpha^2 + m_\beta^2 = 1 \tag{3.23}$$

If the texture consists of lines parallel to $\mathcal{P}_\beta$ (m, $= 0, m_\beta = 1$) or if the lines be on planes passing through the axis (m, $= 1, m_\beta = 0$) then they are symmetric with respect

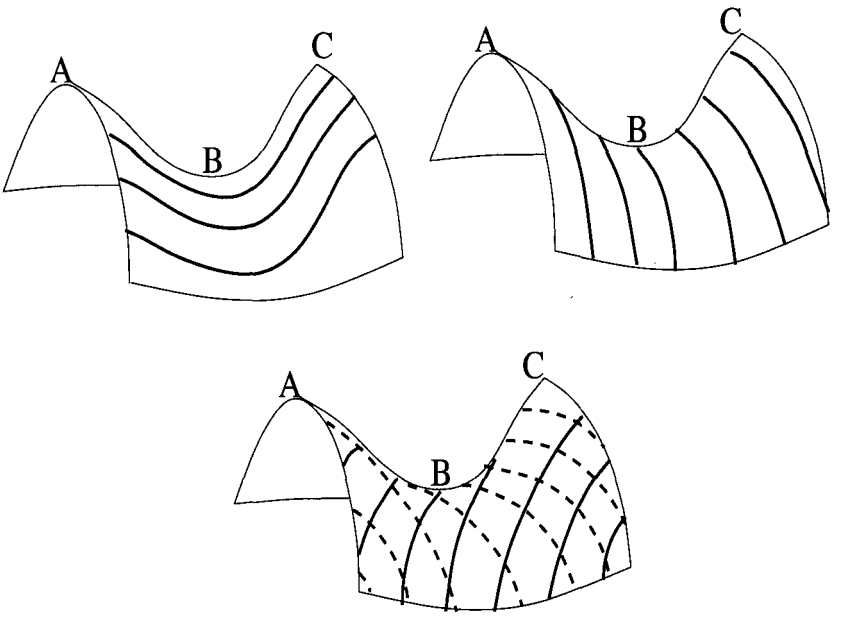

Figure 3.7: Textures (solid lines) on a saddle and their reflection (broken lines) on a mirror that bisects the saddle along the line ABC and is normal to the surface at B.

to reflection on $\mathcal{P}_\alpha$. The chiral part should vanish for these textures, and, extending our knowledge gained from a sphere and a cylinder, we expect the chiral part to be maximum when the lines of $\mathbf{G}$ bisect the angle between $\vec{t_\alpha}$ and $\vec{t_\beta}$. For constant m, and m_β we have

$$c_0^* \gamma_{ij} m^i m^k K_k^j = c_0^* (\frac{1}{R_\alpha} + \frac{\cos a}{R_\beta}) m_\alpha m_\beta \tag{3.24}$$

where R, and R_β are the radii of $\mathcal{C}_\alpha$ and $\mathcal{C}_\beta$ respectively. And

$$k_c(\mathrm{divm})(\mathrm{curlm}) = k_c(\frac{\sin a}{R_\beta})^2 m_\alpha m_\beta \tag{3.25}$$

The chiral part is indeed greatest for $m_\alpha = mg = 1/\sqrt{2}$ and is zero when either component of $\mathbf{G}$ is zero.

3.4 Chirality and budding

We now understand, fairly clearly, the role of chirality in shaping a raft. If k_c is large enough the raft will overcome the elastic resistance to bending and become a spherical bud. Then with increasing values of c_0^* the bud becomes prolate, the pole from which the lines of m radiate drawing farther and farther away from the pole where those lines converge. For sufficiently large c_0^*, the raft takes a flask shape (a cylinder with a spherical cap). In what follows these guesses are corroborated and quantified by variational calculations; before we look at budding, however, it is instructive to observe chiral textures on a plane.

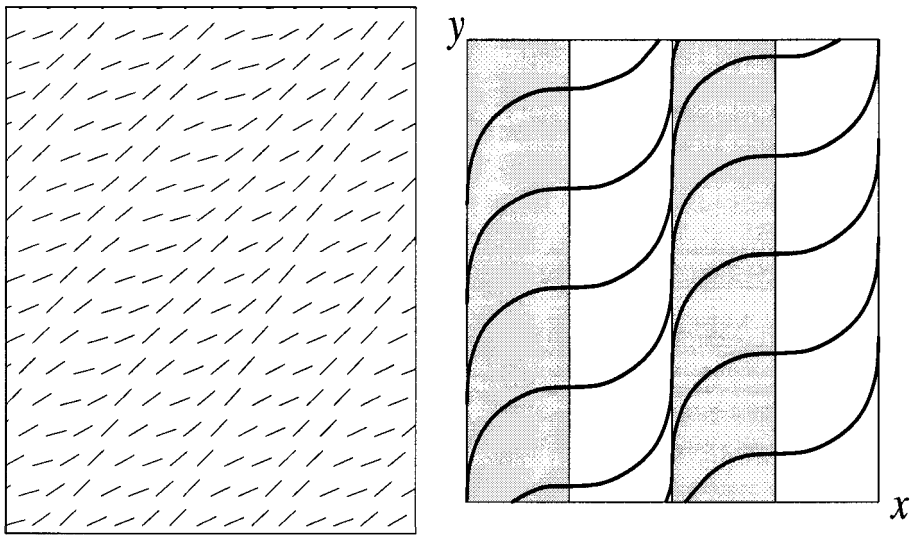

Figure **3.8:** (L) Close up of a texture generated by a monte carlo simulation, and (R) its continuum representation by a mathematical formula. On the shaded portions **div m** is positive and **curl m** is negative, just the reverse on the clear portions.

3.4.1 Simulation on a flat membrane

Let us rewrite the Frank expression as

$$E = L + \int_A 1\,(\mathbf{divm} + \mathbf{curlm})^2 + (k_c - 1)(\mathbf{divm})(\mathbf{curlm}) \tag{3.26}$$

neglecting the curvature of the raft since κ is very large. Naturally the raft would assume a texture with a very high curl and whose divergence is exactly equal and opposite to the curl. We have seen such a texture at the beginning of this chapter — the Archimedes spiral. In polar coordinates, the origin being at the centre of the raft, the spiral described by $\vec{m}$ has constant radial and tangential components everywhere in the raft.

$$m_r^2 + m_\phi^2 = 1 \tag{3.27}$$

$$\mathbf{divm} = \frac{m_r}{r} \tag{3.28}$$

$$\mathbf{curlm} = \frac{m_\phi}{r} \tag{3.29}$$

The texture sought for is $m_r = 1/\sqrt{2}$, $m_\phi = -1/\sqrt{2}$. The energy of this conformation is

$$E = 2\pi R - \pi(k_c - 1)\log(\frac{R}{r_c}) + \epsilon_c \tag{3.30}$$

where R = $A/\sqrt{\pi}$ is the radius of the raft, r_c the radius of the defect core at the centre and ϵ_c is the energy of the defect. The chiral term is infinitely large at the centre of the raft but falls off inversely as the square of the distance from the centre. Is there a texture whose chiral strength is great not just at one point but over the entire raft?

A monte carlo simulation led us to such a solution (Figure **3.8).** Let us place the origin of coordinates on the periphery of the raft and let the x-axis be along a diameter. The

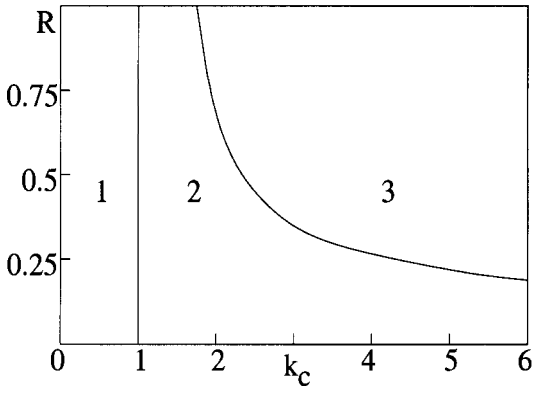

Figure **3.9:** Phases of a raft on a plane **(1)**uniform **(2)** spiral $\epsilon_c = 0, r_c = 0.005$ **(3)** striped $l^* = 0.01$.

texture is parametrised as

$$m_x = |\cos(\frac{x}{l})| \tag{3.31}$$

$$m_y = -|\sin(\frac{x}{l})| \tag{3.32}$$

The texture consists of stripes of width πl parallel to the y-axis. The energy of this conformation is

$$E = 2\pi R + \frac{1}{2l^2} - \frac{k_c}{2l^2}\int_0^{2R} dx\sqrt{2Rx - x^2}|\sin(\frac{2x}{l})| \tag{3.33}$$

The stripes tend to be vanishingly thin ($l \to 0$) in order to minimise the energy; so we arbitrarily set a cut-off l^* on 1.

3.4.2 Implication for a deformable membrane

If κ be finite and if c_0^* vanishes then the raft will be a spherical bud. We have drawn the texture on the bud and parametrised it in the previous sections. If r_0 be the radius of the neck through which the bud is attached to the rest of the membrane then the energy of the raft is

$$E = 2\pi r_0 + \pi\kappa(\frac{\mathrm{R}}{r_{bud}})^2 - \pi(k_c - 1)\int_{\theta_c}^{\pi-\theta_0} d\theta(\frac{\cos^2\theta}{\sin\theta}) + \epsilon_c + \epsilon_k \tag{3.34}$$

where $\theta_c = r_c/r_{bud}$ is the angle subtended by the defect core at the centre of the bud and ϵ_c is the energy of the defect. The area of the raft being a constant we have

$$A = \pi R^2 = 2\pi r_{bud}^2(1 - \cos\theta_0) \tag{3.35}$$

where $\theta_0 = r_0/r_{bud}$ is the angle subtended by the neck at the centre of the bud and ϵ_k is the energy of the neck. If we assume $\epsilon_k = 0$ then our variational calculation suggests that $r_0 \to 0$ because when the neck is infinitesimal the bud has two perfect defects, instead of one, and the effect of chirality is most strongly felt at those points. The assumption of a vanishingly small cost to produce a neck is a safe one; in fluid lipid bilayers the principal

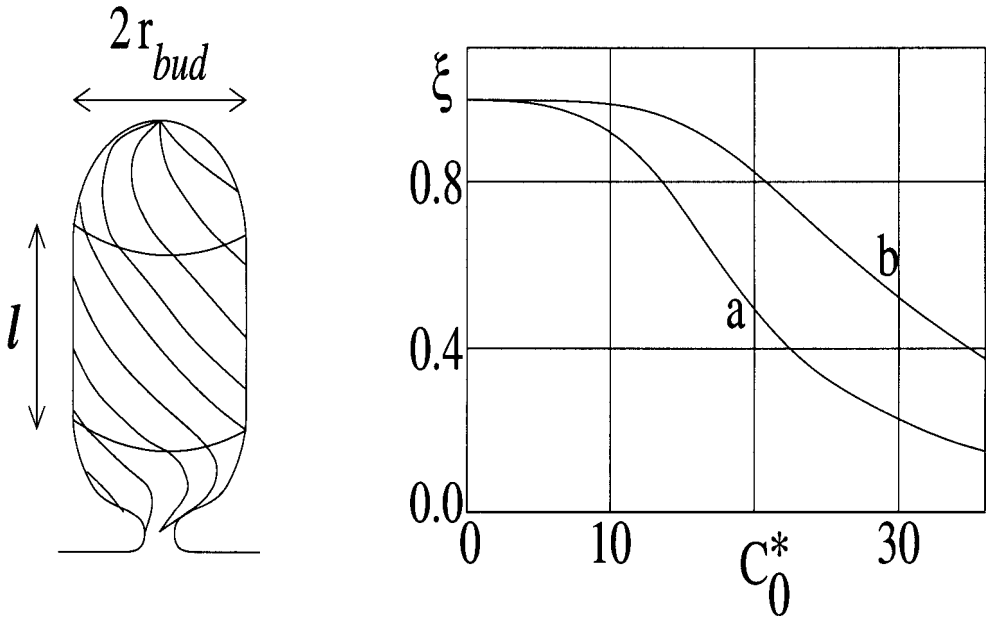

Figure 3.10: (L) Texture of a prolate bud, (R) change in the shape of the bud ($\xi = \frac{2r_{bud}}{2r_{bud}+l}$) with $c_0^* - \kappa = 10$, $k_c = 2$. R = 1 for a, R = 0.5 forb. $\epsilon_c = 0$, $r_c = 0.005$, $\epsilon_k = 0$, $r_0 = 0.005$.

radii of curvature of the saddle-shaped neck (one of them positive, the other negative but both of great magnitude) are so delicately balanced that their sum equals the spontaneous curvature of the membrane and hence the neck costs little energy (Fourcade et al; 1994). As we shall see later, chiral interaction of a vector decorating the neck reduces the cost further.

Comparing Equation 3.33 with Equation 3.29, and noting that the contribution of the chiral terms are roughly equal in the two cases, we find that the bud has less energy than the planar configuration if $2\pi R > 4\pi\kappa$. (We have set $r_0 = 0$.) This is the familiar condition for budding induced by line tension. But there is another piece to the chiral interaction, c_0^*, and this has tremendous potential of creating buds of dimension comparable to that of rafts and clathrin-coated pits found in living cells!

Upon turning c_0^* on, the bud is stretched, the defect being drawn away from the neck. We can model this prolate bud as a cylinder with hemispheres on either side. The texture on the cylinder is the helix we have studied in the previous section; note that the lines of $\vec{m}$ on the cylinder smoothly join the spiral lines of each hemisphere. The energy of this conformation is

$$E = 2\pi r_0 + 2\pi\kappa(1+\cos\theta_0) - \pi(k_c-1)\int_{\theta_c}^{\pi-\theta_0} d\theta(\frac{\cos^2\theta}{\sin\theta}) + \epsilon_c + \epsilon_k \\ +2\pi r_{bud} l(\frac{\kappa}{4r_{bud}^2} - \frac{c_0^*}{2r_{bud}}) \tag{3.36}$$

where 1 is the length of the cylindrical portion of the bud. We have numerically obtained the optimum shape of the bud, the shape minimising this expression of E, of course with

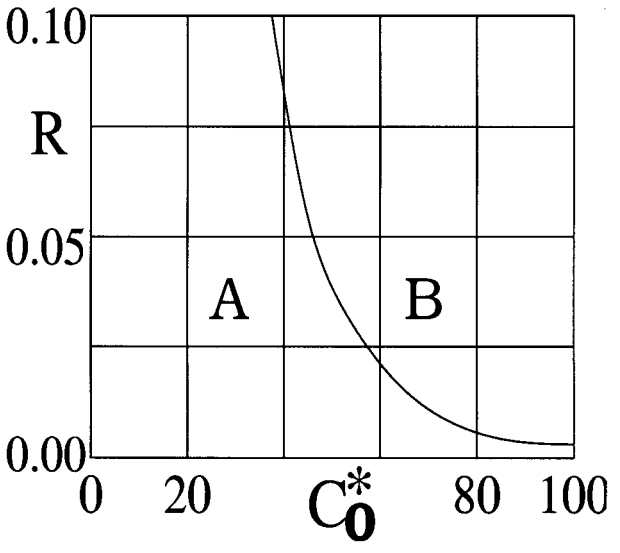

Figure 3.11: Budding due to chirality. $\kappa = 10$, $k_c = 2$. In the region marked A a raft of area A $= \pi R^2$ prefers to be on a plane, while in the region B a bud is the energetically favoured conformation.

the constraint that the area of the bud

$$A = \pi R^2 = 2\pi r_{bud}^2(1 + \cos\theta_0) + 2\pi r_{bud} l \tag{3.37}$$

is constant. The prolateness of the bud, $(2r_{bud} + l)/2r_{bud}$, starts increasing sharply when c_0^* becomes of the order κ/R. Unfortunately we can not prescribe a value of c_0^* for a raft, it has not been measured for any real system, neither a lipid bilayer nor a liquid crystal in bulk. However, we shall attempt a very crude estimate. By introducing a chiral moiety in the acyl chain of a phospholipid, Schnur and his colleagues have observed the spontaneous aggregation of these lipids in a mixture of water and alcohol into hollow tubular structures (approximately 1 μm in diameter) below the chain-melting temperature of the lipid (Schnur et al; 1994). They imagine these tubules to be decorated like a barber's pole by a vector field representing the projection of the rigid chains of the lipid molecules on to the plane of the membrane. The theory developed by Nelson and Powers suggests that the radius of these tubules, $r_{tubule} \sim \frac{\kappa}{c_0^*}$ (Nelson and Powers; 1992). For this system, then, it turns out that $c_0^* \sim 10$. Without any knowledge of the structure of condensed complexes and their interaction with cholesterol, it is impossible to estimate the magnitude of c_0^* in a raft; in all the figures we have drawn we have restricted c_0^*, rather arbitrarily, in the range 0 to 100.

We do not have to worry about the sign of c_0^* as long as it is the same as that of k_c. We have taken k_c and c_0^* everywhere to be positive, had they been negative we would simply reflect the texture shown in Figure 3.10 on a mirror passing through the axis of the raft.

From the phase diagram shown in Figure 3.11 it can be seen that for $\kappa = 10$ and $k_c = 2$, a modest value of $c_0^* = 75$ will make an area with $R = 0.01$ (corresponding to a "real" raft of size 10 nm) pop out of the plane in the form of a bud! As promised, rafts which are too small to have a significant energy of line tension can be fashioned into

buds by the mechanism of chirality. Being a phenomenon of the bulk, budding induced by chirality preempts budding induced by line tension. Thus it seems we have revealed the power that makes a tiny raft enter the cell as if of its own accord — requiring no assistance of the cell cortex or of cytosolic coat proteins: chiral interaction among the condensed complexes floating in the raft could be the hidden source of the power!

3.4.3 Fragmentation of the bud

For a moment let us return to the raft on a plane and suppose that it breaks into n equal parts, each part bearing the same spiral texture. The total area being conserved, each part will be of radius $R/\sqrt{n}$. The total energy of this system is

$$E^{(n)} = 2\pi\sqrt{n}R - n\pi(k_c - 1)\log(\frac{R/\sqrt{n}}{r_c}) + n\epsilon_c \tag{3.38}$$

Since the logarithmic dependence on n is extremely weak, it is obvious that if $E^{(1)}$ be negative then $E^{(n)}$ is more so $(E^{(n)} < E^{(1)} < 0)$. Therefore, under the action of chirality $(k_c > 1)$, the raft is inclined to split.

But, wait a moment. While writing down the expression for the energy of a raft in Equation ***3.5*** did we not presume that the raft has already been assembled from its molecular components, never to be torn apart by any means? If we now wish to calculate $E^{(n)}$ instead of $E^{(1)}$ then we are obliged to include in Equation ***3.5*** terms that account for the interaction of neighbouring molecules in the raft. We are still very far from an understanding of the nature of molecular forces that hold a raft in place (is it hydrogen-bonding? van der Waals forces? hydrophobic shielding? or a combination of all these?). In spite of its shortcoming, we shall carry the argument begun in this section to a conclusion, assuming that forces ordering the $\vec{m}$ field in a raft overpower any other molecular interaction. Even with this assumption Equation ***3.5*** cannot be applied to rafts that are extremely small, higher order terms need to be incorporated. But coefficients of the higher order terms, especially those of chiral origin, are practically impossible to estimate. So let us restrict ourselves to small values of n, trust Equation ***3.5*** the way it stands now, and proceed.

The overriding urge to split is evident in a spherical bud too. Assuming that the sphere is complete (the neck connecting the bud to the parent membrane is infinitesimally thin) we have for n equal parts, each with the same texture, the total energy,

$$E^{(n)} = 4\pi n\kappa - \pi n(k_c - 1)\int_{\theta_c}^{\pi-\theta_c} d\theta(\frac{\cos^2\theta}{\sin\theta}) + 2n\epsilon_c \tag{3.39}$$

For the optimum conformation with $k_c > 1$, $E^{(1)}$ is always negative and $E^{(n)}$ is more so $(E^{(n)} < E^{(1)} < 0)$. Again, the raft is inclined to split.

What is the optimum number of parts (n) of a raft? We cannot address this question. Observe that there is no favoured length scale for chirality — once the chiral strength exceeds a certain threshold, the size of a raft is no longer dictated by the parameters of

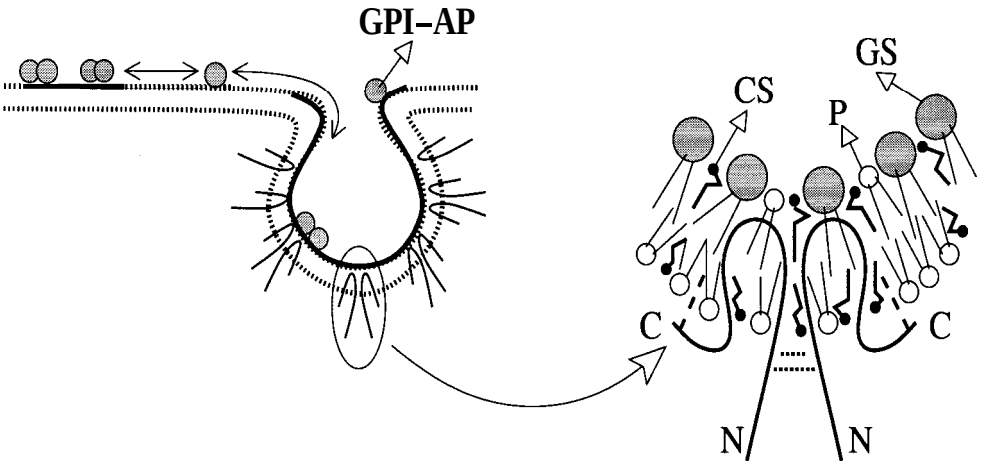

Figure 3.12: (L) Rafts pooled into caveolae. (GPI-AP: GPI-anchored protein) The hair pin structures represent caveolins, their ends are dipped into the cytosol. (R) Close-up of a part of a caveola showing the oligomerisation of caveolins. (CS: cholesterol, GS: glycosphingolipids, P: phospholipids, C: carboxyl terminus, N: amino terminus) Horizontal lines between caveolins represent oligomerisation, broken lines near C represent palmitoylation (Parton and Simons; 1995).

our continuum theory. This is in stark contrast with other modes of budding. Therefore, once we accept the role of chirality in endocytosis, we are forced to view the coat proteins associated with the process of budding in a new light. One of the functions of the coat is to maintain the unity of the bud, overcoming the disruptive agent of chirality. Bare buds, such as those involved in pinocytosis, are minute, chirality not only moulding their shape but also preventing their growth into large structures on the plasma membrane. On the other hand, the elaborate invaginations of the caveolae on the plasma membrane are shaped by chirality into spheres connected by tubules, and the caveolae owe their relatively large size to caveolin, a coat protein nullifying the splitting action of chirality (Figure 3.12).

Caveolae ("small caves") are flask-shaped invaginations of the plasma membrane found in mammalian cells, especially abundant in endothelial cells (lining the interior of blood vessels and other organs). Their size is of the order of 100 nm, nearly an order of magnitude larger than the speculated size of rafts. However molecules associated with rafts are also present in abundance in caveolae (Kurzchalia and Parton; 1999). Furthermore, cells in which caveolae are not normally found can be induced to form these structures by expressing caveolin in them (Fra et al; 1995). Fra and collaborators expressed VIP21-caveolin in a lymphocyte. If the concentration of the protein on the cell membrane crossed a limit then the cell responded by creating stable structures on its surface that bore a striking resemblance to the structure of caveolar pits. Even more remarkably, these structures were able to concentrate GPI-anchored proteins, as was evident by linking the proteins with antibodies!

Caveolins are able to bind cholesterol and glycosphingolipids and thereby stabilise

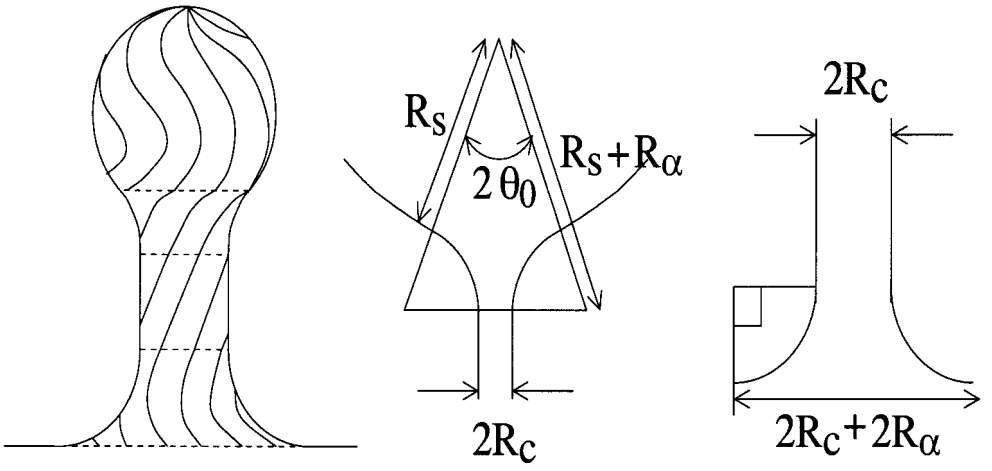

Figure 3.13: (L) The texture of a flask, horizontal lines mark out the two necks (M) geometry of the neck connecting the spherical part of the flask to the cylindrical part (R) geometry of the neck connecting the cylindrical part of the flask to the rest of the membrane.

the caveolar pits — they have an intriguing structure (Parton and Simons; 1995). Both the amino terminus and the carboxyl terminus of these proteins are in the cytosol, a semi-circular domain of thirty three amino acids spans almost the entire thickness of the hydrophobic region of the lipid bilayer. They are palmitoylated (anchored to the membrane by a 16-C saturated fatty acid chain). It has been suggested that the ability of caveolins to bind cholesterol and to oligomerise helps them to detect rafts on the other leaflet and to sequester the rafts into bigger structures (Monier et al; 1996). These observations suggest that caveolae are large aggregations of rafts — but unlike rafts, they are not internalised spontaneously by the cell. Caveolae are stable structures, their internalisation is a regulated process, usually triggered by an extracellular signal (for instance, the simian virus enters a cell by attaching itself to a caveola) (Norkin; 1999).

3.5 Rafts and caveolae

Henceforth we shall assume that the lipid composition of caveolae is so similar to that of rafts that the energy of a caveola is couched in the same Frank expression we have put forward for a raft. Of course the values of the coefficients of chirality, k_c and c_0^*, and the value of the elastic modulus, κ, for a caveola need not be equal to the corresponding values for other forms of rafts; we shall treat these coefficients as variable.

Our aim in this section is to find out the conditions under which a raft, instead of forming a bud, would prefer the shape of a flask. We shall see that, in agreement with experimental observations, the flask shape is more favourable than the bud if (a) the area of the raft (A) is sufficiently great, (b) the membrane is sufficiently stiff, or, in other words, κ is sufficiently great, and (c) c_0^* is sufficiently great. (c) is a necessary condition; even a big and stiff raft can not form a caveola unless c_0^* is large enough.

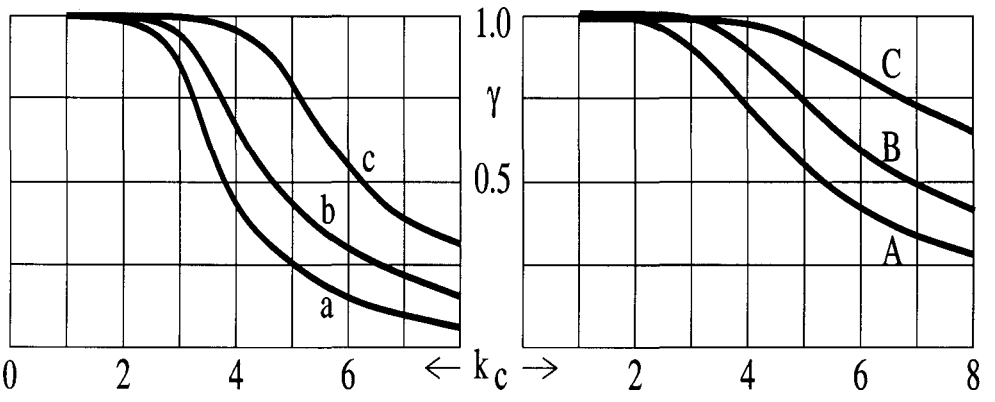

Figure 3.14: Variation of the shape ($\gamma = R_C/R_S$) of a caveola with the chiral coefficients. ($\kappa = 10$, $r_c = 0.05$, $\epsilon_c = 0$). (L) R = 5. a, b and c correspond to the values 40, 50 and 60 of c_0^* respectively. (R) R = 3. **A,** B and C correspond to the values 60, 70 and 80 of c_0^* respectively.

The last condition (c) is the easiest to interpret. We know that a large c_0^* tends to wrap the lines of $\vec{m}$ into a helix around a thin tube. We have seen the effect of this term in the previous section — a spherical bud lengthens into a tubular form upon the action of c_0^*. But. so far we have only dealt with small values of c_0^*; if c_0^* be great then it is much easier to stretch the narrow neck into a tube and decorate it with a helix rather than tampering with the much fatter spherical portion of the bud. The following paragraphs will put these ideas in a quantitative form.

In order to understand the essential features of budding we had ignored the energy (ϵ_k) of the neck joining the bud to the rest of the membrane. We can not do so any more because in a caveola the neck could constitute a sizable portion of the tube that joins the spherical part of the flask to the membrane. So our first task in this section is to model the shape and the texture of the neck and to calculate its energy. Contrary to our first impression, a raft does not necessarily have to incur a cost to produce a neck; in fact, as we will see, for high enough c_0^* a neck is a favoured conformation ($\epsilon_k << 0$).

We model the neck as a saddle. Any plane passing through the axis of the saddle cuts the saddle along a pair of circles, and any cross-section perpendicular to the axis is also a circle. We have described this saddle in a previous section and have seen that the texture favoured by chirality is the one in which the line of $\vec{m}$ at any point bisects the right angle between the transverse and the longitudinal sections of the saddle passing through that point (see Figure 3.7). The neck begins at the smallest cross-section of the saddle (the circle $\mathcal{C}_\beta$ of radius R_β, represented by $\mathrm{a} = 0$) and fans out to the maximum angle $\mathrm{a} = \mathrm{a}_{\max}$ where the radius of the cross-section is $R_\beta + R_\alpha(1 - \cos \mathrm{a}_{\max})$.

A caveola has two necks — the first one connects the spherical part to the cylinder and the second connects the cylinder to the plane of the surrounding membrane (Figure 3.13). The spiral texture of the first neck merges smoothly with the texture of the cylinder on one side and with the texture of the sphere on the other. In a like manner the texture of

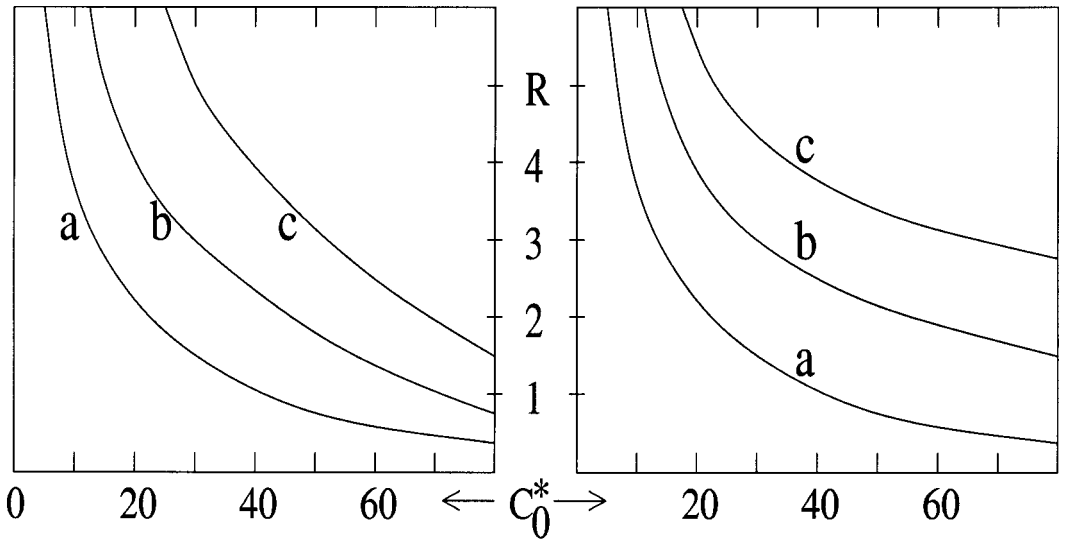

Figure 3.15: Lines separating the two phases of the raft — to the left of each curve is the bud phase, and to the right is the flask phase. (L) $\kappa = 10$. a, b and **c** correspond to the values 2, 5 and 8 of k_c respectively. (R) $k_c = 2$. **a,** b and **c** correspond to the values 10, 20 and 30 of κ respectively. (In every case r, $= 0.05$ and $\epsilon_c = 0$.)

the second neck merges smoothly with that of the cylinder.

The first neck subtends an angle θ_0 at the centre of the sphere, therefore $\alpha^{(1)}_{max} = \theta_0$. And $R^{(1)}_\beta = R_C$, the radius of the cylinder. If R_S be the radius of the sphere then

$$\theta_0 = \arcsin\left(\frac{R_C + R^{(1)}_\alpha}{R_S + R^{(1)}_\alpha}\right) \tag{3.40}$$

The energy of this neck is

$$\begin{aligned}\epsilon^{(1)}_k = \frac{\pi}{2}\kappa \Bigg[&\left(1 + \frac{R_C}{R^{(1)}_\alpha} + \frac{3}{2}\frac{R^{(1)}_\alpha}{R_C} + \frac{1}{2}\left(\frac{R^{(1)}_\alpha}{R_C}\right)^2\right)\theta_0 - \left(3 + 2\frac{R^{(1)}_\alpha}{R_C} + \left(\frac{R^{(1)}_\alpha}{R_C}\right)^2\right)\sin\theta_0 \\ &+ \frac{1}{4}\frac{R^{(1)}_\alpha}{R_C}\left(3 + \frac{R^{(1)}_\alpha}{R_C}\right)\sin 2\theta_0 + \frac{1}{3}\left(\frac{R^{(1)}_\alpha}{R_C}\right)^2 \sin^3\theta_0\Bigg] \\ -\pi(k_c - 1)\left(\frac{R^{(1)}_\alpha}{R_C}\right) &\left[\frac{1}{2}\left(1 + \frac{R^{(1)}_\alpha}{R_C}\right)\theta_0 - \frac{1}{4}\left(1 + \frac{R^{(1)}_\alpha}{R_C}\right)\sin 2\theta_0 - \frac{1}{3}\left(\frac{R^{(1)}_\alpha}{R_C}\right)\sin^3\theta_0\right] \\ -\pi c_0^* R^{(1)}_\alpha &\left[\left(1 + \frac{R_C}{R^{(1)}_\alpha} - \frac{1}{2}\frac{R^{(1)}_\alpha}{R_C}\right)\theta_0 + \frac{R^{(1)}_\alpha}{R_C}\sin\theta_0 - \frac{1}{4}\left(\frac{R^{(1)}_\alpha}{R_C}\right)\sin 2\theta_0\right]\end{aligned} \tag{3.41}$$

and its area

$$A^{(1)}_k = 2\pi R^{(1)}_\alpha \left[(R^{(1)}_\alpha + R_C)\theta_0 - R^{(1)}_\alpha \sin\theta_0\right] \tag{3.42}$$

If the second neck has to join the caveola smoothly with a flat surrounding membrane then we must have $\alpha^{(2)}_{max} = \pi/2$, and as we had before, $R^{(2)}_\beta = R_C$. This creates a periphery of length $2\pi(R^{(2)}_\alpha + R_C)$ through which the surrounding membrane interacts with the caveolar pit. The energy of the neck is

$$\epsilon^{(2)}_k = \frac{\pi}{2}\kappa\left(\frac{\pi}{2}\frac{R_C}{R^{(2)}_\alpha} + \left(\frac{3\pi}{4} - 2\right)\frac{R^{(2)}_\alpha}{R_C} + \left(\frac{\pi}{4} - \frac{2}{3}\right)\left(\frac{R^{(2)}_\alpha}{R_C}\right)^2 + \frac{\pi}{2} - 3\right) \tag{3.43}$$

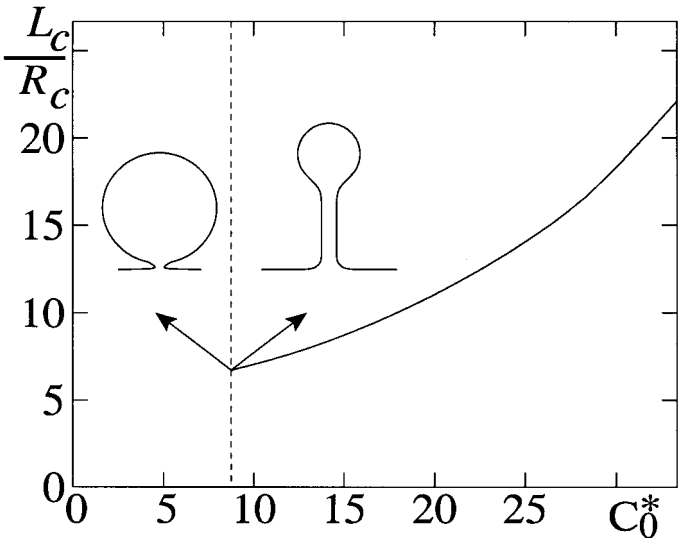

Figure 3.16: Discontinuity of the transition from the bud to the flask. $k_c = 2$, R = 5. To the left of the broken line $L_C = 0$, so the optimum shape is a bud. The profiles of the raft, drawn to scale, show the optimum shapes just to the left and just to the right of the broken line.

$$-\pi(k_c-1)(\frac{R_\alpha^{(2)}}{R_C})(\frac{\pi}{4}+(\frac{\pi}{4}-\frac{1}{3})\frac{R_\alpha^{(2)}}{R_C})-\pi c_0^* R_\alpha^{(2)}(\frac{\pi}{2}+\frac{\pi}{2}\frac{R_C}{R_\alpha^{(2)}}+(1-\frac{\pi}{4})\frac{R_\alpha^{(2)}}{R_C})$$
$$+2\pi(R_\alpha^{(2)}+R_C)$$

and its area

$$A_k^{(2)} = 2\pi R_\alpha^{(2)}\left[(\frac{\pi}{2}-1)R_\alpha^{(2)}+\frac{\pi}{2}R_C\right] \tag{3.44}$$

Denoting the length of the cylindrical part by L_C and the radius of the spherical part by R_S, we finally arrive at the total energy of the system.

$$E = \epsilon_k^{(2)} + 2\pi R_C L_C(\frac{\kappa}{4R_C^2}-\frac{c_0^*}{2R_C})+\epsilon_k^{(1)} \tag{3.45}$$
$$+2\pi\kappa(1+\cos\theta_0)-\pi(k_c-1)\int_{\theta_c}^{\pi-\theta_0}d\theta(\frac{\cos^2\theta}{\sin\theta})+\epsilon_c$$

We have numerically obtained the optimum shape of the caveola (the values of R_S, R_C, $R_\alpha^{(1)}$, $R_\alpha^{(2)}$ and L_C that minimise E), always satisfying the constraint of the conservation of area.

$$\mathrm{A} = \pi R^2 = A_k^{(1)} + A_k^{(2)} + 2\pi R_S^2(1+\cos\theta_0) + 2\pi R_C L_C \tag{3.46}$$

The different shapes we have found for the caveola fall into two classes — (A) the shape of a bud, where the spherical part is attached to the parent membrane without any cylindrical bridge ($L_C = 0$), and (B) the shape of a flask, where the spherical bud is held apart from the parent membrane by a cylinder ($L_C > 0$). In every bud we find that $R_\alpha^{(1)} << R_S$ and $R_\alpha^{(2)} << R_S$; in every flask $R_\alpha^{(1)} << R_S$ and $R_\alpha^{(2)} << L_C$. Therefore the necks are narrow and the shape of the flask is almost wholly determined by the dimensions of the spherical and the cylindrical parts.

For fixed values of R and k_c there is a threshold of c_0^* that has to be crossed to get into the flask shape, any smaller value will produce only a bud. The threshold value of c_0^* increases with increase in k_c or decrease in R, as shown in Figure **3.15.** The transition from the bud to the flask is not a smooth one. Keeping R and k_c fixed, as we increase the value of c_0^* from zero, we find that L_C jumps discontinuously from zero to a finite value as c_0^* crosses the threshold (Figure **3.16).**

Since the lipid and sterol composition of the membrane varies little from one raft to another, or even between a raft and a caveola, we expect the values of the chiral coefficients for the different microdomains to vary within a narrow margin. Given a fixed pair of values of k_c and c_0^*, we have a minimum size, R_{min}, for a raft to be in the shape of a flask. Observations of cells with caveolae support our theoretical prediction of the existence of a minimum size of a flask.

We would also like to know how the stiffness of the membrane governs the shape of a raft. The covering of the inner leaflet of a caveola with caveolin, a protein that oligomerises and binds to the cholesterol of the membrane and whose hydrophobic region spans the thickness of the membrane, will certainly increase the effective value of κ for the bilayer. As a result the caveolar pit will become bigger. From Figure **3.15** it can be seen that for fixed values of k_c and c_0^*, the minimum size of a raft capable of taking the shape of a flask (R_{min}) increases with K.

We may now take a step ahead and ask: instead of being in the shape of a flask (a bulb with a tubular stalk), can a caveola take the form of a string of spherical bulbs connected by a system of tubules? We know that if the area of the domain becomes sufficiently large then a competition would ensue between the two chiral properties, k_c and c_0^*: the first would like to produce spheres, bunching the lines of $\vec{m}$ into tight spirals toward the poles, and the other would prefer long cylinders wrapped in a helical texture. It is fruitful to ask how the area of the domain partitions into the two conformations.

We extend the parametrisation of the flask shape to include spheres $(S_1, S_2, S_3, ...)$ connected to cylinders $(T_1, T_2, T_3, ...)$ by saddles $(N_1, N_2, N_3, ...)$ and the whole structure

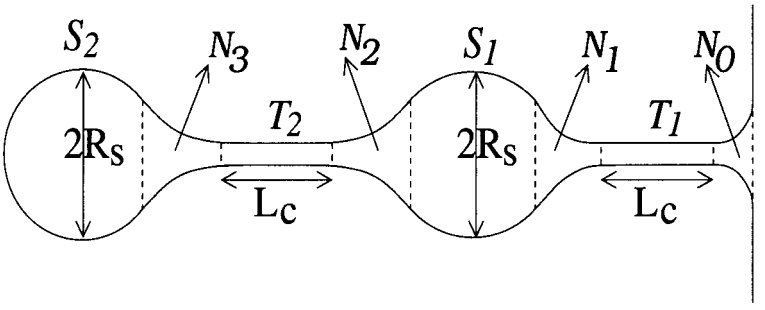

Figure **3.17:** Shape of a caveola attached to the surrounding membrane by the neck N_0 and consisting of two bulbs, each of radius R_S, and two identical tubules, each of length L_C. The necks N_1, N_2 and N_3, connecting the tubules with the bulbs are geometrically identical.

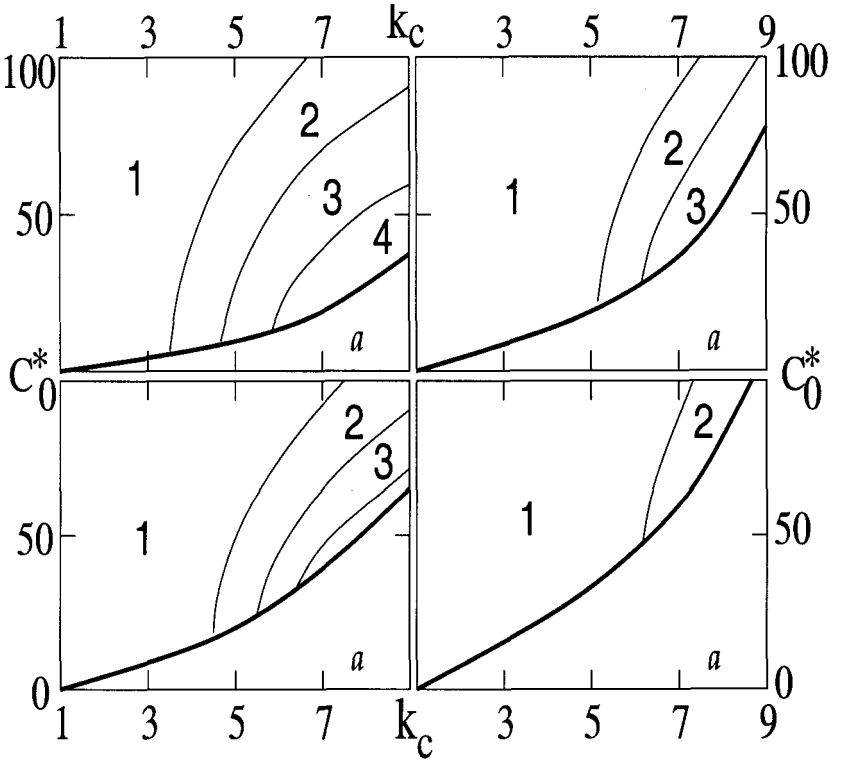

Figure 3.18: Optimum shape of a caveola with n bulbs connected by n tubules. The label **(1, 2, 3)** in each region of a graph refers to the optimum value of n, while in the region marked a there is no tubule. (TL) R = 5, $\kappa = 10$ (TR) R = 5, $\kappa = 20$ (BL) R = 3, $\kappa = 10$ (BR) R = 3, $\kappa = 20$.

joins with the rest of the membrane through the neck N_0 (Figure 3.17). Each of these components is robed in exactly the same texture as we have described for the flask-shaped caveola. For simplicity we take all the tubules to be of the same dimension (length L_C and radius R_C), all the bulbs to be of the same radius (R_S), and all the necks except N_0, the one at the base, to be of the same outer radius (R,) and the same inner radius ($R_\beta = R_C$).

The results of the variational calculation (displayed in Figure 3.18) bear out our expectations. Given a pair of values of k_c and c_0^*, the bigger the domain and the less stiff it is the more the number of bulbs and tubules will it sprout. While for a fixed size and a fixed elastic modulus of the domain, the greater is c_0^* the fewer the number of bulbs and the longer the tubules joining them. There is a threshold that c_0^* must cross in order for the domain to have any tubular part at all — any smaller value of c_0^* leads to the result $L_C = 0$ and the domain takes the form of a necklace of spheres connected by infinitely narrow necks. The multitude of spherical buds is simply the result of the splitting proclivity of chirality that we have described in the previous section, we shall not deal with it here.

The plasma membrane of skeletal muscle cells develop long and slender invaginations that surround each myofibril inside the cell. These invaginations, called the transverse

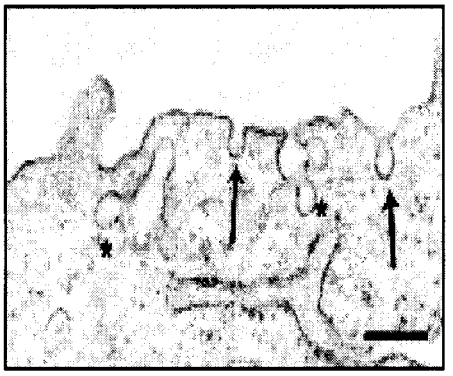

Figure **3.19:** An electron micrograph of caveolae (scale bar — 200 nm). They can exist as single caveolae (arrows) or as chains of multiple caveolae (asterisks). Caveolae are linked to the periphery of the cell, the identity of the Y-shaped tubular structure inside the cell is not clear (van Deurs et al; 2003).

tubules, serve to relay the signal from the motor neuron rapidly to the sarcolemmal vesicles around each myofibril and thus induce a simultaneous shortening of all the fibres in the cell (Parton et al; 1997). Parton and his collaborators, after an investigation of the biogenesis of the transverse tubules, have arrived at the observation that these intriguing structures develop from large aggregations of caveolae! They have studied the distribution of caveolin in a muscle cell and have found that caveolin is restricted to the sarcolemmal membranes in a fully developed muscle cell but large patches of the plasma membrane are associated with caveolin in a growing cell. These patches take the shape of bulbs connected by tubules (like bunches of grapes) and give rise to the intricate system of transverse tubules in the mature muscle (Figure 3.19).

3.6 Appendix

3.6.1 Formula for the calculation of energy

Any point on the surface of the membrane is specified by the vector $\vec{R}(x)$ where x = (x^1, x^2) forms a two dimensional manifold. The tangent plane at any point on the surface is defined by the covariant vectors

$$\vec{e_a} = \frac{\partial \vec{R}}{\partial x^a} \tag{3.47}$$

where $a = 1, 2$. The metric tensor is

$$g_{ab} = \vec{e_a} \cdot \vec{e_b} \tag{3.48}$$

An element of the surface bounded by the sides dx^1 and dx^2 is

$$dA = \sqrt{g} dx^1 dx^2 \tag{3.49}$$

$$g = det g_{ab} \tag{3.50}$$

With the help of the metric tensor and its inverse, we can convert any covariant tensor, $\vec{e_a}$ for instance, into its contravariant form:

$$\vec{e^a} = g^{ab}\vec{e_b} \tag{3.51}$$

$$g^{ab}g_{bc} = \delta^a_c \tag{3.52}$$

A vector field, $\mathbf{G}$, on the tangent plane, is defined by the covariant tensor, m_a, where

$$\vec{m} = m_a\vec{e^a} \tag{3.53}$$

$\vec{N}$ is the unit normal to the surface and the curvature tensor

$$K_{ab} = \vec{N} \cdot \frac{\partial^2 \vec{R}}{\partial x^a \partial x^b} \tag{3.54}$$

For any scalar field, ϕ, we can easily construct a covariant tensor as its gradient.

$$\mathbf{grad}\phi = \frac{\partial \phi}{\partial x^a}\vec{e^a} \tag{3.55}$$

In order to calculate the divergence of a vector field, $\vec{m}$, however, we have to use the covariant derivative, D, of $\vec{m}$.

$$\mathbf{div}\vec{m} = D_a m^a \tag{3.56}$$

$$D_a m^c = \frac{\partial m^c}{\partial x^a} + \Gamma^c_{ab} m^b \tag{3.57}$$

$$\Gamma^c_{ab} = \vec{e^c} \cdot \frac{\partial \vec{e_b}}{\partial x^a} \tag{3.58}$$

Similarly, the curl of $\vec{m}$ is given by

$$\mathbf{curl}\vec{m} = \gamma^a_c D_a m^c \tag{3.59}$$

where γ_{ab} is the completely antisymmetric pure covariant tensor.

We can now use this formula to calculate the quantities in the expression of the energy of the raft on a spherical, cylindrical or a saddle-like surface, all the surfaces being parametrised by the coordinates introduced in section **3.3.** For a sphere,

$$g_{11} = r^2, g_{12} = 0, g_{21} = 0, g_{22} = r^2 \sin^2\theta \tag{3.60}$$

$$K^1_1 = \frac{1}{r}, K^2_1 = 0, K^1_2 = 0, K^2_2 = \frac{1}{r} \tag{3.61}$$

$$\mathbf{div}\vec{m} = \frac{1}{r}\frac{\partial m_\theta}{\partial \theta} + \frac{1}{r\sin\theta}\frac{\partial m_\phi}{\partial \$} + (\frac{\cot\theta}{r})m_\theta \tag{3.62}$$

$$\mathbf{curl}\vec{m} = \frac{1}{r}\frac{\partial m_\phi}{\partial \theta} - \frac{1}{r\sin\theta}\frac{\partial m_\theta}{\partial \$} + (\frac{\cot\theta}{r})m_\phi \tag{3.63}$$

For a cylinder,

$$g_{11} = r^2, g_{12} = 0, g_{21} = 0, g_{22} = 1 \tag{3.64}$$

$$K^1_1 = \frac{1}{r}, K^2_1 = 0, K^1_2 = 0, K^2_2 = 0 \tag{3.65}$$

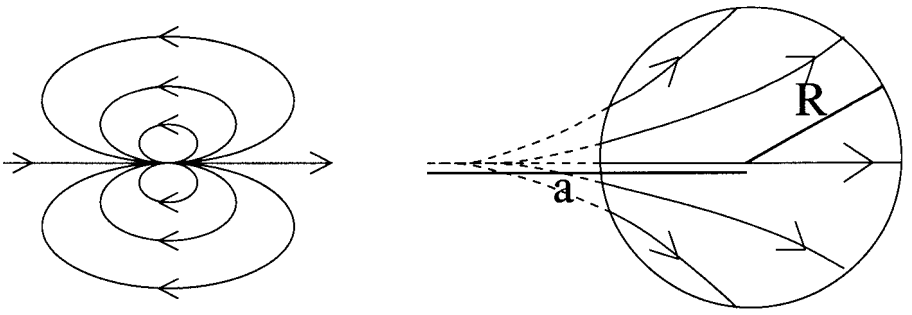

Figure 3.20: Effect of anisotropic line tension on the texture of an achiral circular domain. (L) a boojum of charge 2; (R) texture of a domain of radius R whose centre is at a distance a from the core of the boojum.

$$\mathbf{div}\vec{m} = \frac{1}{r}\frac{\partial m_\phi}{\partial \phi} + \frac{am_r}{\partial x} \tag{3.66}$$

$$\mathbf{curl}\vec{m} = \frac{1}{r}\frac{\partial m_z}{\partial \phi} - \frac{\partial m_\phi}{\partial z} \tag{3.67}$$

And for a saddle

$$g_{11} = R_\alpha^2, g_{12} = 0, g_{21} = 0, g_{22} = R_\beta^2 \tag{3.68}$$

$$K_1^1 \equiv \frac{1}{R_\alpha}, K_1^2 \equiv 0, K_2^1 \equiv 0, K_2^2 = -\frac{\cos \mathbf{a}}{R_\beta} \tag{3.69}$$

$$\mathbf{div}\vec{m} = \frac{1}{R_\alpha}\frac{dm_\alpha}{\partial \alpha} + \frac{1}{R_\beta}\frac{\partial m_\beta}{\partial \beta} + \frac{\sin \alpha}{R_\beta} m_\alpha \tag{3.70}$$

$$\mathbf{curl}\vec{m} = \frac{1}{R_\alpha}\frac{\partial m_\beta}{\partial \alpha} - \frac{1}{R_\beta}\frac{dm_\alpha}{\partial \beta} + \frac{\sin \alpha}{R_\beta} m_\beta \tag{3.71}$$

3.6.2 Conformation of a planar achiral raft

We shall now study the shape and texture of a planar domain of area A that does not have any chiral interaction in the bulk ($k_c = 0$). The energy of this domain is

$$E = \sigma_0 L + \int_A \frac{k_1}{2}(\mathbf{div}\vec{m})^2 + \frac{k_2}{2}(\mathbf{curl}\vec{m})^2 + \sigma_1 \mathbf{div}\vec{m} + \sigma_2 \mathbf{curl}\vec{m} \tag{3.72}$$

where L is the perimeter of the domain. σ_1 and σ_2, the coefficients of spontaneous bend and spontaneous splay respectively, are in fact the components of an anisotropic line tension:

$$\int_A \sigma_1 \mathbf{div}\vec{m} = \sigma_1 \oint_L \vec{m} \cdot \vec{n} \tag{3.73}$$

$$\int_A \sigma_2 \mathbf{curl}\vec{m} = \sigma_2 \oint_L \vec{m} \cdot \vec{t} \tag{3.74}$$

$\vec{t}$ and $\vec{n}$ are respectively the unit tangent and the unit normal to the perimeter of the domain, both being on the plane of the domain. Pettey and Lubensky have shown that

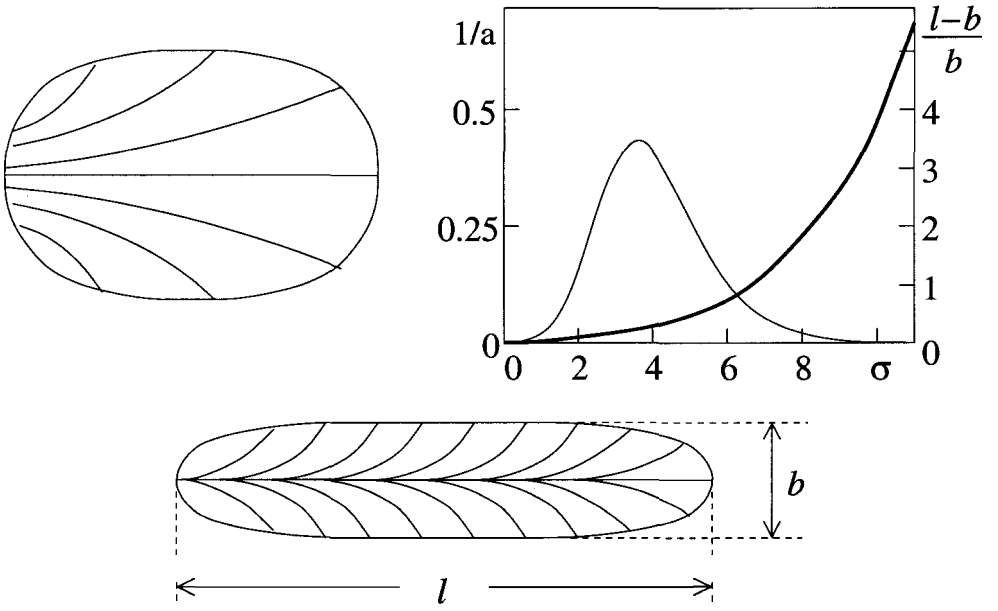

Figure 3.21: Stretching action of strong anisotropic line tension. (TR) variation of $\frac{1}{a}$ with a for a domain of effective radius R = 1 (thin line), and variation of the prolateness $\frac{l-b}{b}$ of the same domain with a (thick line). (TL) and (B) show the conformation of the domain for a = 6.5 and a = 9.5 respectively.

the optimum texture for any pair of values of σ_1 and σ_2 can be obtained from the texture minimizing the energy

$$E = \sigma_0 L - \sigma \oint_L \vec{m} \cdot \vec{n} + \int_A \frac{k_1}{2} (\mathbf{div}\vec{m})^2 + \frac{k_2}{2} (\mathbf{curl}\vec{m})^2 \tag{3.75}$$

$$\sigma = \sqrt{\sigma_1^2 + \sigma_2^2} \tag{3.76}$$

by rotating $\vec{m}$ at every point through a fixed angle (Pettey and Lubensky; 1999). As a result, in spite of the spontaneous splay being a chiral term, the domain can never assume a chiral conformation in the absence of a chiral interaction in its bulk.

$\vec{m}$ can be represented by the angle ϕ it makes with a fixed axis passing through the centre of the domain. If we set $k_1 = k_2 = k$ then the energy of the domain is in the form

$$E = \sigma_0 L - \sigma \oint_L \vec{m} \cdot \vec{n} + \frac{k}{2} \int_A |\mathbf{grad}\phi|^2 \tag{3.77}$$

Any texture that is a local minimum of this energy must satisfy the laplace equation

$$\nabla^2 \phi = 0 \tag{3.78}$$

Obviously, if a = 0 then $\vec{m}$ will everywhere aim in the same direction to minimise the energy of the domain and the solution sought for is $\phi = 0$ (or any fixed angle). If a does not vanish then

$$\phi(r, 0) = N\theta + c_1 r \sin 0 + c_2 r^2 \sin 20 + c_3 r^3 \sin 30 + \ldots \tag{3.79}$$

The resulting texture is a boojum of charge N whose core is at the origin of coordinates (Figure 3.20). In order to specify the shape (R) of the domain let us temporarily shift the origin from the core of the boojum by a distance a to the centre of the domain.

$$\mathcal{R}(\theta) = R_0(1 + \alpha_1 \cos 0 + \alpha_2 \cos 20 + \alpha_3 \cos 30 + ...) \tag{3.80}$$

0 varies from 0 to 2π. Since the area of the domain has to be A, we must have

$$\pi R_0^2 + \frac{\pi}{2}(\alpha_1^2 + \alpha_2^2 + \alpha_3^2 + ...) = A = \pi R^2 \tag{3.81}$$

We set our units of length and energy to make $k = 1$ and $\sigma_0 = 1$; then, for given values of R and a, minimise the energy as a function of the parameters N, a, c_1, c_2, c_3, ... ,α_1, α_2, α_3, ...

The best value of N is always 2. We also find that including terms in the texture with coefficients c_n, whose n exceeds 1, reduces the minimum value of E by at most 1%(Sarasij and Rao; 2002). So we parametrise the texture in the simpler form

$$\phi = 2\theta + c_1 y \tag{3.82}$$

where y is the distance of any point from the axis of the domain. As a is increased from 0, the core of the boojum approaches the centre of the domain but the domain remains almost circular. As a is raised beyond a threshold the core begins to recede from the centre and the domain bulges out at the equator (Figure 3.21). For large values of a it is a good approximation to set $\phi = c_1 y$ and take the domain to be a rectangular block bracketted at the equator by two semicircular caps.